https://doi.org/10.3311/PPme.38385

Periodica Polytechnica Mechanical Engineering, 69(1), pp. 23–31, 2025

Unsteady Magneto-radiative Flow of Copper-water Nanofluid Over an Exponentially Stretching Surface

Khodani Sherrif Tshivhi[1*], Maashutha Samuel Tshehla[1]

[1] Department of Mathematics, Faculty of Military Science, Stellenbosch University, 7395 Saldanha, P.O.B. X2, South Africa
[*] Corresponding author, e-mail: tshivhi@sun.ac.za

Received: 23 September 2024, Accepted: 27 January 2025, Published online: 04 February 2025

Abstract

Understanding the complex behavior of fluid flows under various physical influences is crucial for advancing engineering and industrial applications. This paper presents the investigation of the unsteady, incompressible, single-phase magneto-radiative flow of a copper-water nanofluid over an exponentially stretching surface, considering the effects of viscous dissipation and temperature-dependent heat sources. This model, proposed in the present analysis, is based on fundamentals of the continuity and Navier–Stokes equations with mass conservation. Further, use of a similarity transformation will reduce the equations to dimensionless form and provide a numerical solution using the Runge–Kutta–Fehlberg method. In physics, engineering, and industrial applications, the most interesting parameters are the velocity, temperature, skin friction, and the Nusselt number (*Nu*). The results of this study are compared with previous works, showing significant agreement with findings under similar conditions. The analysis reveals that both temperature and velocity boundary layer increase when all very specific effects of radiation (*R*), heat source (*Q*), copper nanoparticle volume fraction, and magnetic field strength parameter are present. On the other hand, it is found that skin friction increases when considering both copper nanoparticle volume fraction and magnetic field strength parameter, but the *Nu* decreases if *R*, *Q*, copper nanoparticle volume fraction, and magnetic field strength parameter are the factors responsible for that. These outcomes will be further delineated through graphics and be elaborated in engineering and industrial context.

Keywords

magneto-radiative flow, copper-water nanofluid, viscous dissipation, exponentially stretching surface, similarity transformations, Runge–Kutta–Fehlberg method, temperature-dependent heat sources

1 Introduction

The reality that comes with the application of viscous fluid over a stretching surface is the most fundamental part of many engineering and industrial processes, including cooling the metallic sheets, oceanography, paper production, plastic sheet extrusion, artificial fibers, polymer industries, and aerodynamics. Conventional approaches to heat transfer have been getting insufficient in the view of technological improvements and miniaturization. As a result, the utilization of naonofluid has become the most suitable heat transfer technique that is inspired by Choi's classic research innovation [1]. Choi's groundbreaking concept has significantly increased research in the fields of physics and applied mathematics. As demonstrated in the research by Li et al. [2], Ganvir et al. [3], Tshivhi [4], Monaledi [5], Bachok et al. [6], and Mukhopadhyay et al. [7], heat transfer using nanofluids proves to be more effective than traditional methods.

Abbas and Hayat [8] analyzed the characteristics of heat transfer of viscous fluid over a nonlinear stretching surface by studying steady, incompressible two-dimensional stagnation slip flow. They have obtained the analytical solution using homotopy analysis. Goyal and Bhargava [9] studied the effects of Brownian motion, thermophoresis and cross-diffusion in triple-diffusive boundary layer flow of binary nanofluid over a nonlinear stretching sheet. They employed group theory transformations to reduce the partial differential equation into an ordinary differential equation. They finally solved the model problem by the variation finite element method. Ibrahim and Gadisa [10] studied nonlinear convective flow considering heat generation or absorption and a chemical reaction in Eyring-Powell nanofluid using the Catteneo–Christov model over a stretching surface. They employed the Galerkin finite

Cite this article as: Tshivhi, K. S., Tshehla, M. S. "Unsteady Magneto-radiative Flow of Copper-water Nanofluid Over an Exponentially Stretching Surface", Periodica Polytechnica Mechanical Engineering, 69(1), pp. 23–31, 2025. https://doi.org/10.3311/PPme.38385

element method to get the solution. The main finding was that a higher chemical reaction rate increases the mass transfer rate and simultaneously decreases the heat transfer rate, while local buoyancy acts in the opposite way. Tshivhi and Makinde [11] discussed the effects of surface slipperiness, magnetic field, dissipation on heat transfer and nanoparticles volume fraction in nanofluid flow over a linearly stretching shrinking surface. The numerical solution for nonlinear boundary value problem obtained by Runge–Kutta and shooting methods; they found that dual solutions exist for certain range of parameters in a case of shrinking surface. Fang [12] considers the steady two-dimensional laminar flow over a continuously shrinking sheet with a power-law surface velocity and mass transfer in a quiescent fluid. Solutions were obtained for some mass transfer parameters to be double, and among other findings was the result of velocity overshoot near the wall and at the boundary layer edge for some solution branches. The flow driven by wedge velocity, transpiration parameter, and fluid power law and past a permeable stretching surface has been analyzed in steady, two-dimensional, and laminar conditions by Postelnicu and Pop [13]. The Runge–Kutta scheme coupled with a standard shooting technique has been employed to determine the existence of dual solutions. Stability investigation showed that solution branches with a lower value are unstable while the upper branch solution is stable.

Jalil et al. [14] treated a nonlinear boundary layer flow problem with a power-law fluid over a power-law stretching surface. They obtained an analytical solution for the problem using a perturbation method and presented behavior analysis. From their results, one can observe that a decrease in the nonlinear parameter "n" leads to a reduction of both the boundary layer thickness and skin friction coefficient. In Mustafa et al. [15], heat transport efficiency in the boundary layer flow of a power-law fluid along a moving permeable wedge was studied. As indicated by their result, the velocity of dilatant fluid decreases close to the wedge surface and reaches its maximum far away from the wedge surface. Shah et al. [16], on the other hand, studied the flow of sodium alginate-alumina/copper hybrid nanofluids towards a stretching/shrinking sheet with slip in power law form numerically and taking into account suction. It was determined that the solutions are in some range of shrinking sheets. Moreover, increasing the thermal slip factor in both the solutions decreased the thickness of the thermal boundary surface. Ahmed et al. [17] analyzed the power-law behavior in the stagnation point flow of radiative magneto Jeffrey fluid with slip. It was noted that adding Jeffery's material and slip parameters increased the numerical value of the coefficient of skin friction. Al-hanaya et al. [18] studied the combined dilatant, pseudo-plastic and Newtonian nanofluids' flow due to a flow along truncated cones by a set of nonsimilar solutions via finite differences analyses. Results showed that, relative to dilatant nanofluids, the temperature and nanoparticles distributions are higher for pseudo-plastic nanofluids. However, with regard to the heat and mass transfer rates, it is exactly opposite: the dilatant nanofluids provided higher rates compared to pseudo-plastic nanofluids.

A thorough literature review has revealed a significant gap in the current research [19–25]: the need for for comprehensive analysis of the combined effects of radiation, heat sources, and magnetic fields on nanofluid boundary layer flow over an exponentially stretching surface. Addressing this gap is crucial for engineers and researchers looking to optimize system performance, enhance process efficiency, and ensure safety across various engineering applications.

This study offers a novel approach by analyzing the unsteady magneto-radiative flow of copper-water nanofluid over an exponentially stretching surface, a topic that has yet to be fully explored in existing research.

Building upon the foundational work of Kaur et al. [26], which examined the effects of viscous dissipation and temperature-dependent thermal conductivity in a porous flat channel, our study uniquely integrates these factors into the context of exponentially stretching surfaces. This allows for new insights into the complex dynamics of fluid flows influenced by viscous dissipation and temperature-dependent heat sources.

Our objective is to advance the understanding of fluid boundary layer flow from linear to exponential stretching surfaces, taking into account the combined influences of radiation, heat sources, and magnetic fields. We achieve this by developing a comprehensive model based on fundamental fluid dynamics principles, transforming the equations into their dimensionless form using the Blasius similarity method, and solving them numerically through the Runge–Kutta–Fehlberg integration scheme. This approach promises to offer fresh perspectives on fluid flow behavior and its practical applications.

2 Model formulation

This study examines the single-phase, incompressible, unsteady boundary layer flow of copper-water nanofluid over an exponential surface with slip, as shown in Fig. 1.

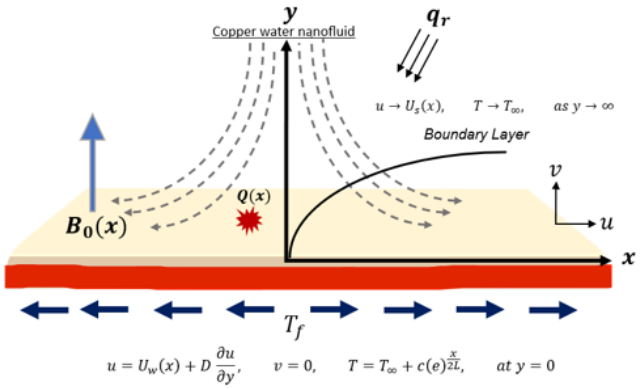

Fig. 1 Illustration depicting the model problem

The x-axis lies along the flat surface, while the y-axis is normal to it. In this study, we assume that the base fluid and nanoparticles are at thermal equilibrium. The velocity of the exponential stretching surface (U_w), is with the free-stream velocity (U_s). The surface temperature is (T_f), and the free-stream temperature is (T_∞). The flow encounters an external magnetic flux of intensity (B_0), which is applied perpendicular to the nanofluid motion. It also involves non-uniform internal heat generation/absorption (Q^*) and thermal radiation (q_r). The modified governing boundary layer equations for continuity, momentum, and energy are provided as [8, 19, 20]:

$$\frac{\partial u}{\partial x}+\frac{\partial v}{\partial y}=0, \tag{1}$$

$$\frac{\partial u}{\partial t}+u\frac{\partial u}{\partial x}+v\frac{\partial u}{\partial y} = U_s\frac{dU_s}{dx}+\frac{\mu_{nf}}{\rho_{nf}}\left(\frac{\partial^2 u}{\partial y^2}\right)-\frac{\sigma_{nf}}{\rho_{nf}}\left(B_1\right)^2\left(u-U_s\right), \tag{2}$$

$$\frac{\partial T}{\partial t}+u\frac{\partial T}{\partial x}+v\frac{\partial T}{\partial y}=\frac{k_{nf}}{\left(\rho C_p\right)_{nf}}\frac{\partial^2 T}{\partial y^2} +\frac{\mu_{nf}}{\left(\rho C_p\right)_{nf}}\left(\frac{\partial u}{\partial y}\right)^2+\frac{Q^*(x)}{\left(\rho C_p\right)_{nf}}\left(T-T_\infty\right) -\frac{1}{\left(\rho C_p\right)_{nf}}\frac{\partial q_r}{\partial y}+\frac{\sigma_{nf}}{\left(\rho C_p\right)_{nf}}\left(B_1\right)^2\left(u-U_s\right)^2. \tag{3}$$

Conditions at the exponential stretching surface ($y = 0$):

$$u=U_w(x)+D\frac{\partial u}{\partial y}, \quad v=0,\ T=T_\infty+\frac{c}{(1-\varphi t)}(\exp)^{\frac{x}{2L}}, \tag{4}$$

Conditions at free stream ($y \to \infty$):

$$u \to U_s(x),\ T \to T_\infty. \tag{5}$$

The expression of the skin friction coefficient (C_f) and the local Nusselt number (Nu) at the exponential stretching surface are defined as:

$$C_f=\frac{\tau_w}{\rho_f U_s^2},\ Nu=\frac{2Lq_w}{k_f\left(T_f-T_\infty\right)}. \tag{6}$$

The parameters in Eqs. (1) to (6) are expressed as:

$$B_1=\frac{B_0(\exp)^{\frac{x}{2L}}}{\sqrt{(1-\varphi t)}},\ U_s=\frac{a(\exp)^{\frac{x}{L}}}{(1-\varphi t)},\ U_w=\frac{b(\exp)^{\frac{x}{L}}}{(1-\varphi t)}, \quad T_f=T_\infty+\frac{c(\exp)^{\frac{x}{2L}}}{(1-\varphi t)},\ Q(x)=\frac{Q_0(\exp)^{\frac{x}{L}}}{(1-\varphi t)}, \tag{7}$$

$$D=\frac{d(\exp)^{\frac{-x}{2L}}}{(1-\varphi t)},\ \tau_w=\left[\mu_{nf}\frac{\partial u}{\partial y}\right]_{y=0},\ q_w=-k_{nf}\frac{\partial T}{\partial y}|_{y=0}, \quad q_r=-\frac{4\sigma^*}{3k^*}\frac{\partial T^4}{\partial y},\ T^4\approx 4T_\infty^3T-3T_\infty^4, \tag{8}$$

where T^4 is the temperature (T) just is rised to the power of 4.

Refer to the nomenclature above for the definition of parameters and subscripts. In analyzing radiation, we assume that the temperature fluctuations within the flow are minimal, which allows us to approximate the T^4 term in Eq. (8) as a linear function of temperature. This approximation is made by employing a truncated Taylor series expansion centered at the T_∞. To convert the modeled partial differential Eqs. (1) to (6) into ordinary differential equations, we employed a similarity transformation by defining the similarity variables as follows:

$$\psi=(\exp)^{\frac{x}{2L}}\sqrt{\frac{2\nu_f La}{(1-\varphi t)}}f(\eta), \quad \eta=y(\exp)^{\frac{x}{2L}}\sqrt{\frac{a}{2\nu_f L(1-\varphi t)}},\ T=\frac{\theta c(\exp)^{\frac{x}{2L}}}{(1-\varphi t)}+T_\infty, \tag{9}$$

$$u=\frac{a(\exp)^{\frac{x}{L}}}{(1-\varphi t)}f'(\eta), \quad v=-(\exp)^{\frac{x}{2L}}\sqrt{\frac{\nu_f a}{2L(1-\varphi t)}}\left(f(\eta)+\eta f'(\eta)\right). \tag{10}$$

By using the stream function (ψ) to satisfy the continuity Eq. (1), where as $u = \partial\psi/\partial y$ and $v = -\partial\psi/\partial x$, and applying the similarity transformation, we arrive at the following ordinary differential equation:

$$\begin{aligned} &A_1\left(2-2f'(\eta)-\eta f''(\eta)\right)-2f'(\eta)f'(\eta)\\ &+f(\eta)f''(\eta)+2+A_2A_3f'''(\eta)\\ &-A_3A_4A_5\left(f'(\eta)-1\right)=0, \end{aligned} \tag{11}$$

$$\begin{aligned} &-2A_1\theta(\eta)-2A_1\eta\theta'(\eta)-f'(\eta)\theta(\eta)\\ &+f(\eta)\theta'(\eta)+\frac{A_3A_6A_7}{\mathrm{Pr}}\theta''(\eta)\\ &+A_2A_3A_7\mathrm{Ec}f'(\eta)^2+A_3A_7Q\theta(\eta)\\ &-\frac{4A_3A_7R}{3\mathrm{Pr}}\theta''(\eta)+A_3A_4A_5A_7\mathrm{Ec}\left(f'(\eta)-1\right)^2=0. \end{aligned} \tag{12}$$

With the conditions at exponential stretching surface and free stream given as:

$$\begin{aligned} &f'(0)=\lambda+\beta f''(0),\ f(0)=0,\\ &\theta(0)=1,\ f'(\infty)=1,\ \theta(\infty)=0. \end{aligned} \tag{13}$$

The ordinary differential form of the expression of the skin C_f and the local Nu at the exponential stretching surface are defined as:

$$C_f\sqrt{\mathrm{Re}}\sqrt{\frac{2L}{x}}=A_2f''(0),\ \frac{Nu}{\sqrt{\mathrm{Re}}}\sqrt{\frac{2L}{x}}=-A_6\theta'(0). \tag{14}$$

The parameters in Eqs. (11) to (14) are defined in the nomenclature and expressed as:

$$A_1=\frac{L\varphi}{a},\ A_2=\frac{\mu_{nf}}{\mu_f},\ A_3=\frac{\rho_f}{\rho_{nf}},\ A_4=\frac{\sigma_{nf}}{\sigma_f}, \tag{15}$$

$$A_5=\frac{2LB_0^2\sigma_f}{a\rho_f},\ A_6=\frac{k_{nf}}{k_f},\ A_7=\frac{C_{pf}}{C_{pnf}},\ \mathrm{Pr}=\frac{\mu_fC_{pf}}{k_f}, \tag{16}$$

$$\mathrm{Ec}=\frac{U_s^2}{C_{pf}\left(T_f-T_\infty\right)},\ Q=\frac{2LQ_0}{a\left(\rho C_p\right)_f},\ R=\frac{4\sigma^*T_\infty^3}{k_fk^*}. \tag{17}$$

In Table 1, we present the values of density, specific heat capacity, thermal conductivity, and electrical conductivity for the base fluid (water) and nanoparticles (copper), as obtained from the literature by Yang et al. [21],

Table 1 Nanoparticles and base fluid thermophysical properties [6, 21, 22]

Properties	Water	Copper
Density (kg/m^3)	999.7	8933.0
Specific heat capacity (j/kg K)	4179	385
Thermal conductivity ($W/m\ k$)	0.613	401
Electrical conductivity × 10^{-6} (S/m)	5.5	59.6

Table 2 The interaction between base fluids and nanoparticles [23–26]

Properties	Nanofluid
Density	$\rho_{nf}=(1-\phi)\rho_f+\phi\rho_s$
Heat capacity	$\left(\rho C_p\right)_{nf}=(1-\phi)\left(\rho C_p\right)_f+\phi\left(\rho C_p\right)_s$
Viscosity	$\frac{\mu_{nf}}{\mu_f}=\frac{1}{(1-\phi)^{2.5}}$
Thermal conductivity	$\frac{k_{nf}}{k_f}=\frac{\left(k_s+2k_f\right)-2\phi\left(k_f-k_s\right)}{\left(k_s+2k_f\right)+\phi\left(k_f-k_s\right)}$
Electrical conductivity	$\frac{\sigma_{nf}}{\sigma_f}=1+\frac{3\left(\frac{\sigma_s}{\sigma_f}-1\right)\phi}{\left(\frac{\sigma_s}{\sigma_f}+2\right)-\left(\frac{\sigma_s}{\sigma_f}-1\right)\phi}$

Muhammad et al. [22], Bachok et al. [6]. The properties of the nanofluid were calculated using the expressions in Table 2, based on the literature by Mandal and Mukhopadhyay [23], Ghosh and Mukhopadhyay [24], Hamid et al. [25] and Kaur et al. [26].

3 Numerical procedure

The ordinary differential Eqs. (11) to (13) are transformed into an initial value problem, defined as:

$$\begin{aligned} &x_1=f(\eta),\ x_2=f'(\eta),\ x_3=f''(\eta),\\ &x_4=\theta(\eta),\ x_5=\theta'(\eta),\ x_1'=x_2,\ x_2'=x_3, \end{aligned} \tag{18}$$

$$\begin{aligned} &2x_2^2-A_1\left(2-2x_2-\eta x_3\right)\\ &x_3'=\frac{-x_1x_3-2+A_3A_4A_5\left(x_2-1\right)}{A_2A_3},\ x_4'=x_5, \end{aligned} \tag{19}$$

$$\begin{aligned} &2A_1x_4+2A_1\eta x_5+x_2x_4-x_1x_5-A_2A_3A_7\mathrm{Ec}x_3^2\\ &x_5=\frac{-A_3A_7Qx_4-A_3A_4A_5A_7\mathrm{Ec}\left(x_2-1\right)^2}{\frac{A_3A_7}{\mathrm{Pr}}\left(A_6-\frac{4R}{3}\right)}. \end{aligned} \tag{20}$$

The corresponding initial conditions are:

$$\begin{aligned} &x_1(0)=0,\ x_2(0)=\beta x_3(0)+\lambda,\\ &x_3(0)=b_1,\ x_4(0)=1,\ x_5(0)=b_2, \end{aligned} \tag{21}$$

To solve the equations, we will first use the shooting method by guessing initial values for (b_1) and (b_2). We will solve Eqs. (18) to (21) with the Runge–Kutta method. If the solution fails to converge to the desired boundary conditions, we will utilize the Newton–Raphson method to refine our guesses for (b_1) and (b_2). The equations will then be resolved, and the results will be plotted for further analysis.

4 Results and discussion

The result obtained was compared with those of Ishak [27] and Mohd Nasir et al. [28] under the specific condition

Table 3 Comparison of the value of local skin friction

λ	Ishak [27]	Mohd Nasir et al. [28]	Present results
0.0	1.232588	1.232588	1.232588
0.1	1.146561	1.146561	1.146561
0.2	–	1.051130	1.051130
0.5	0.713295	0.713295	0.713295
1	0	0.0	0.0
2	−1.887307	−1.8873295	−1.88731

where all parameters were set to zero, except for the effect of surface slipperiness, which was allowed to vary as shown in comparison Table 3.

For the computations of the results in this analysis, the following parameters values were held constant: unsteadiness (A_1) = 0.2, magnetic field (A_5) = 0.3, Prandtl number (Pr) = 6.2, Eckert number (Ec = 0.2), heat source (Q) = 0.2, surface slipperiness (β) = 0.1, stretching (λ) = 0.2, and radiation (R) = 0.1. As can be seen in Fig. 2, with an increase in the A_5 strength parameter, the flow of copper-water nanofluid starts increasing. This is because an increase in A_5 strength enhances the Lorentz force, increasing internal friction and viscous dissipation that resist the nanofluid flow, bringing about an increase in the kinetic energy and a drop in temperature of nanofluids in the boundary layer. Moreover, both the velocity and temperature boundary layer thicknesses move closer to the surface. Fig. 3 illustrates that as the nanoparticle parameter (ϕ) increases, both velocity and temperature rise simultaneously. This occurs because the presence of nanoparticles boosts the nanofluid's density and viscosity, resulting in higher fluid velocity. Additionally, nanoparticles enhance thermal conductivity, which increases the

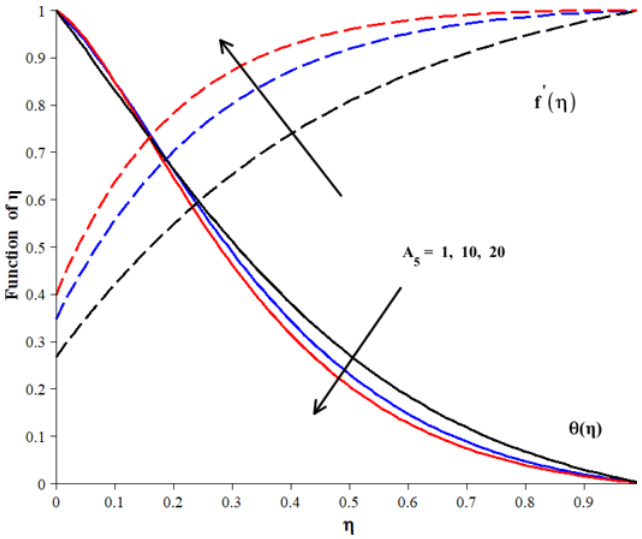

Fig. 2 Velocity and temperature boundary layer with the effect of A_5

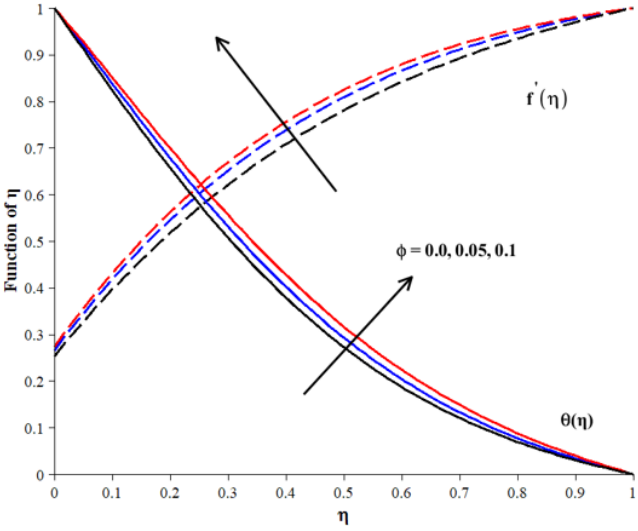

Fig. 3 Velocity and temperature boundary layer with the effect of ϕ

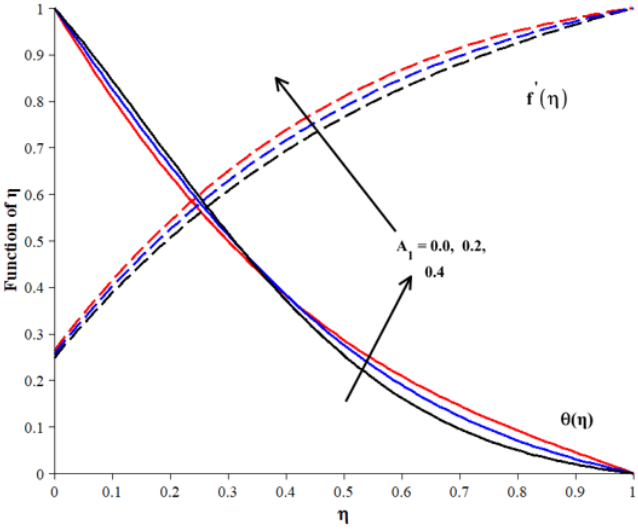

Fig. 4 Velocity and temperature boundary layer with the effect of A_1

temperature within the boundary layer and causes it to thicken. Fig. 4 illustrates that increasing the A_1 parameter in the velocity profile leads to an increase in velocity. This is due to the flow becoming turbulent, which introduces oscillations or instabilities in the velocity distribution. Meanwhile, the temperature profile becomes unstable, near the surface, the temperature decreases, but further away from the surface, the temperature increases. This behavior is attributed to the unsteady flow, which causes the temperature boundary layer to shift closer to the surface. Fig. 5 shows that as the R parameter increases, the temperature decreases. This occurs because conductive heat transfer becomes more dominant over radiative heat transfer, causing the temperature boundary layer to contract and move closer to the surface. As the Q parameter increases, the fluid temperature rises due to the additional thermal energy generated within the nanofluids shown

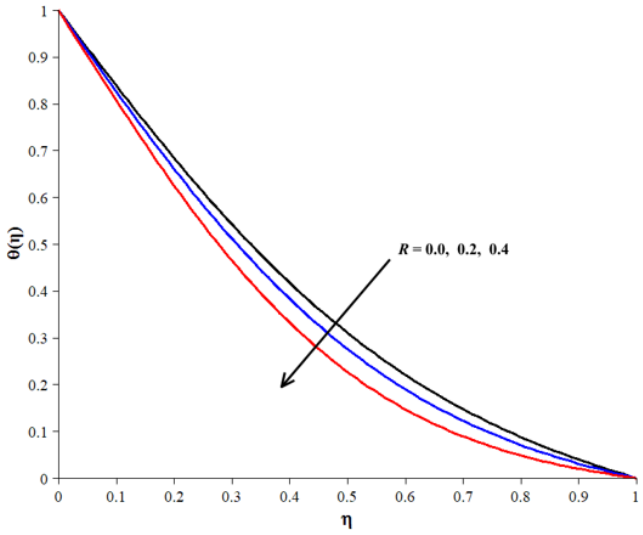

Fig. 5 Temperature boundary layer with the effect of R

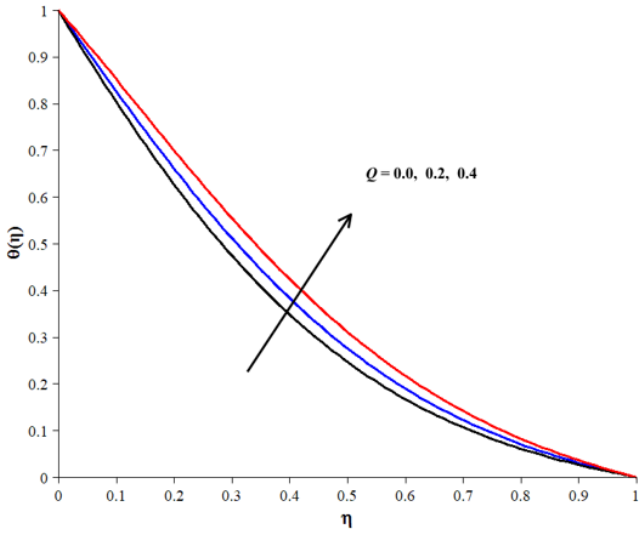

Fig. 6 Temperature boundary layer with the effect of Q

in Fig. 6. This rise in temperature can cause the thermal boundary layer to thicken, pushing the boundary layer farther away from the surface.

Table 4 presents the percentage changes in velocity and temperature resulting from various parameter influences. When considering the effect of R alone, the temperature decreases by 24%. In contrast, Q alone causes the temperature to rise by 11%. The effect of copper nanoparticle volume fraction (ϕ) results in a 5% increase in temperature and a 4% increase in fluid velocity. With A_5 alone, the temperature decreases by 0.01%, while the velocity increases by 0.01%. When evaluating the combined effects of R, Q, copper nanoparticle fraction (ϕ), and A_5, the temperature increases by 6%, and the velocity rises by 5%. Understanding these combined effects and optimizations is crucial for ensuring safe operation in applications involving exponential stretching surfaces.

Table 4 Impact of parameters in the velocity and temperature profiles

R	Q	ϕ	A_5	Velocity ($f'(\eta)$)	Change in velocity (%)	Temperature ($\theta'(\eta)$)	Change in temperature (%)
0	0	0	0	0.7014	–	0.3829	–
0.4	0	0	0	0.7014	–	0.2877	−24%
0	0.4	0	0	0.7014	–	0.4525	+11%
0	0	0.05	0	0.7323	+4%	0.4009	+5%
0	0	0	0.2	0.7078	+0.01%	0.3824	−0.001%
0.4	0.4	0.05	0.2	0.7378	+5%	0.4038	5%

Fig. 7 illustrates the effects of parameter variations of A_1, A_5 strength, and nanoparticle volume fraction (ϕ) on the skin friction. It is evident that skin friction increases as the values of these parameters rise. This increase is attributed to the heightened nanofluid velocity, which creates a steep velocity gradient near the surface, thereby increasing the shear stress at the wall and enhancing skin

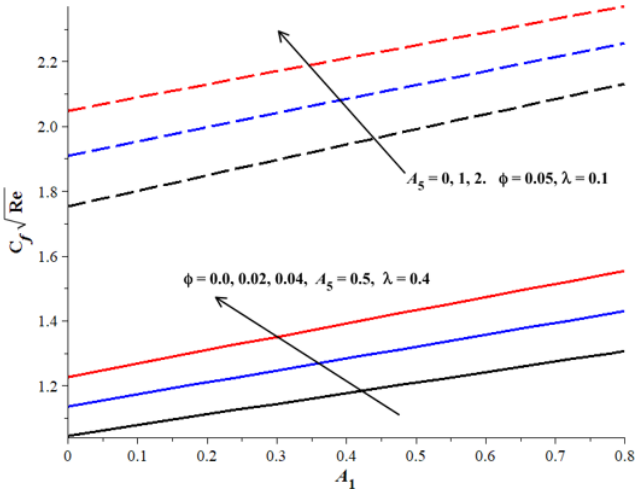

Fig. 7 Skin friction effect on the boundary layer surface

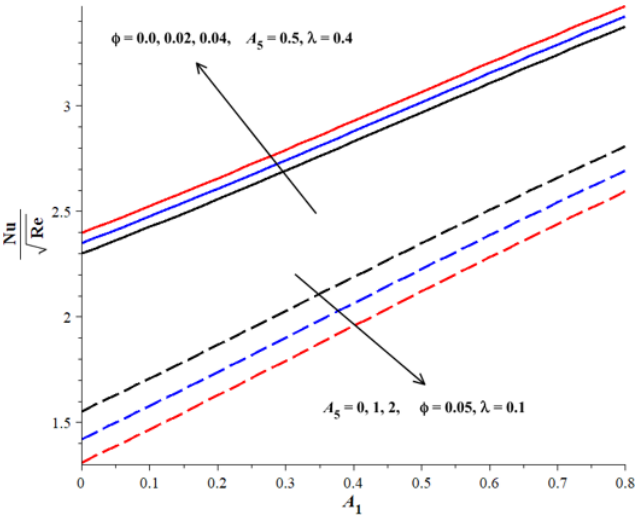

Fig. 8 Effect of A_1 and ϕ on the Nu

friction. Additionally, the increased viscosity of copper-water nanoparticles contributes to greater skin friction by further raising the shear stress near the surface. From Fig. 8, it is clear that an increase in A_1 and ϕ values makes the *Nu* larger, that is, the convective heat transfer rate is improved in relation to the conductive heat transfer rate. That is, a further increase in A_5, on the other hand, leads to a decline in the *Nu*. This decrease is to a great extent due to the fact that with the rise of the A_5 strength, the convective heat transfer rate in comparison with conductive heat transfer rate tends to shrink. Finally, Fig. 9 shows that as the *R* parameter increases, the *Nu* also tends to rise. This happens because, as the *R* parameter gets larger, radiative heat transfer becomes more significant in the overall heat transfer process. It helps transfer heat away from the surface, even in areas where convection alone might not be as effective.

The results from Figs. 7 to 9 are seen to be confirmed by Table 5. It is found that the skin friction is raised by

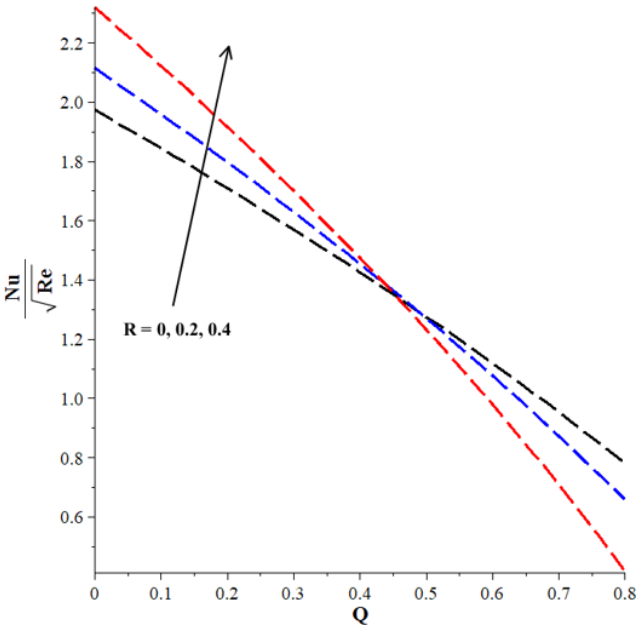

Fig. 9 Effect of *R* on the *Nu*

Table 5 Impact of parameters in the skin friction and temperature profiles

R	*Q*	ϕ	A_5	Skin friction ($f'(\eta)$)	Change in velocity (%)	*Nu* ($\theta'(\eta)$)	Change in temperature (%)
0	0	0	0	1.5022	–	1.9085	–
0.4	0	0	0	1.5022	–	2.4407	+28%
0	0.4	0	0	1.5022	–	1.3810	−28%
0	0	0.05	0	1.8476	+23%	2.0248	+6%
0	0	0	0.2	1.5319	+2%	1.8899	−1%
0.4	0.4	0.05	0.2	1.8787	+25%	1.5292	−20%

23% when using only 5% copper nanoparticles. On the contrary, by means of the A_5 parameter alone, the skin friction increased by 2%. When both copper nanoparticle volume faction (ϕ) and A_5 are considered together, skin friction rises by 25%. For the *R* parameter, it alone causes a 28% increase in the *Nu*, whereas the *Q* parameter alone would be a 28% decrease. The copper nanoparticle volume fraction (ϕ) itself leads to a heat transfer increase of 6% and A_5 alone further decreases the *Nu* by 1%. When all the effects of *R*, *Q*, copper nanoparticle volume fraction (ϕ), and A_5 are taken into account, the *Nu* decreases by 20%. The investigation and optimization of these physical parameters skin friction and the *Nu* are the major factors which would ensure the highest performance of the system under exponential stretching scenarios.

5 Conclusion

The paper examines the unsteady magneto-radiative flow of a copper-water nanofluid over an exponentially stretching surface, incorporating the effects of viscous dissipation and temperature-dependent *Q*s and sinks. The partial differential model was developed and transformed into dimensionless equations using similarity transformations. The solution was then obtained using the Runge–Kutta–Fehlberg integration scheme. The key findings are as follows:

- The velocity of the fluid growing is proportional to parameters associated with A_1, A_5 and copper nanoparticle volume fraction.
- The temperature of the fluid increases with the increase of parameters A_1, *Q*, and copper nanoparticle volume fraction, and decreases with higher parameters values of A_5 and *R*.
- Skin friction on the wall is growing with the higher values of A_1, A_5 and copper nanoparticle volume fraction.
- The *Nu* increases with the parameter value of A_1, *R*, and *Q* and also decreases with the increase of A_5.
- The temperature increases by 6% and the velocity rises by 5% if all unique effects of R, Q, copper nanoparticle volume fraction, and A5 are present.
- Considering both copper nanoparticle volume fraction and A5 together, skin friction rises by 25%, while the *Nu* decreases by 20% when all effects of *R*, *Q*, copper nanoparticle volume fraction, and A_5 are accounted for.

The study's findings have significant practical implications for industries that depend on fluid dynamics and heat transfer, such as electronics, energy systems,

and manufacturing. For instance, increasing the copper nanoparticle volume fraction and applying a A_5 can enhance fluid velocity and temperature, thereby improving heat dissipation in systems like cooling devices and heat exchangers. However, this improvement comes at the cost of higher skin friction, which can increase energy consumption and lead to greater maintenance requirements, especially in components such as pumps or turbines. Moreover, achieving a balance between heat transfer efficiency and A_5 strength is crucial. While a stronger A_5 can enhance certain properties, it may also reduce the *Nu*, thereby diminishing heat transfer performance. These findings provide valuable guidance for engineers, enabling them to design more efficient systems by optimizing parameters such as nanoparticle concentration and A_5 strength. By doing so, they can improve thermal management, reduce operational costs, and extend the lifespan of critical components.

Nomenclature

u, v	Velocity components
x, y	Cartesian coordinates
T_f	Temperature of hot fluid
T_∞	Temperature at free stream
U_w	Velocity at the surface
U_s	Velocity at the free stream
a, b, c, d, φ, b_1, b_2	Constant
τ_w	Surface shear stress
q_w	Surface heat flux
L	Reference length
D	Slip factor
B_0	External uniform magnetic field
B_1	Applied magnetic field B_0 is proportion to square root (SQRT) $(1-\varphi \times t)$
C_f SQRT(Re) SQRT($2L/x$)	Local skin friction coefficient
Nu/SQRT(Re) × SQRT($2L/x$)	Local Nusselt friction coefficient
μ_{nf}	Nanofluid dynamic viscosity
ρ_{nf}	Density of the nanofluid
σ_{nf}	Electrical conductivity of the nanofluid
σ	Electrical conductivity of the base fluid
T	Temperature
k_{nf}	Thermal conductivity of the nanofluid
C_{pnf}	Specific heat capacity of the nanofluid
C_p	Specific heat capacity of the base fluid
q_r	Radiative heat flux
ρ_f	Density of the base fluid
k_f	Thermal conductivity of the base fluid
σ^*	Stefan-Boltzmann constant
k^*	Mass absorption coefficient
η	Dimensionless surface length
$\theta'(\eta)$	Dimensionless temperature
$f'(\eta)$	Dimensionless velocity
ψ	Stream function
A_5	Magnetic field parameter
Ec	Eckert number parameter
Q	Heat source parameter
Q_0	Uniform internal heat generation/absorption
Pr	Prandtl number parameter
R	Radiation parameter
β	Surface slipperiness parameter
λ	Stretching parameter
Re	Reynold's number
ϕ	Copper nanoparticle volume fraction
v_f	Kinematic viscosity
t	Time
A_1	Unsteadiness parameter
A_2	Viscosity of nanofluid
A_3	Density of nanofluid
A_4	Electrical conductivity of nanofluid
A_6	Thermal conductivity of nanofluid
A_7	Specific heat capacity of nanofluid

References

[1] Choi, S. U. S. "Enhancing Thermal Conductivity of Fluids with Nanoparticles", ASME Fluids Engineering Division, 66, pp. 99–105, 1995.

[2] Li, J., Zhang, X., Xu, B., Yuan, M. "Nanofluid research and applications: A review", International Communications in Heat and Mass Transfer, 127, 105543, 2021. https://doi.org/10.1016/j.icheatmasstransfer.2021.105543

[3] Ganvir, R. B., Walke, P. V., Kriplani, V. M. "Heat transfer characteristics in nanofluid—A review", Renewable and Sustainable Energy Reviews, 75, pp. 451–460, 2017. https://doi.org/10.1016/j.rser.2016.11.010

[4] Tshivhi, K. S. "Entropy generation analysis and optimization of cooling systems in industrial and engineering operations", Heat Transfer, 53(2), pp. 733–754, 2024. https://doi.org/10.1002/htj.22968

[5] Monaledi, R. L. "Theoretical Study of Variable Viscosity Nanofluids Flow in Microchannels", PhD Thesis, Stellenbosch University, 2020.

[6] Bachok, N., Ishak, A., Pop, I. "Boundary layer stagnation-point flow and heat transfer over an exponentially stretching/shrinking sheet in a nanofluid", International Journal of Heat and Mass Transfer, 55(25–26), pp. 8122–8128, 2012. https://doi.org/10.1016/j.ijheatmasstransfer.2012.08.051

[7] Mukhopadhyay, S., Bhattacharyya, K., Layek, G. C. "Mass Transfer over an Exponentially Stretching Porous Sheet Embedded in a Stratified Medium", Chemical Engineering Communications, 201(2), pp. 272–286, 2014. https://doi.org/10.1080/00986445.2013.768236

[8] Abbas, Z., Hayat, T. "Stagnation slip flow and heat transfer over a nonlinear stretching sheet", Numerical Methods for Partial Differential Equations, 27(2), pp. 302–314, 2011. https://doi.org/10.1002/num.20523

[9] Goyal, M., Bhargava, R. "Numerical study of thermodiffusion effects on boundary layer flow of nanofluids over a power law stretching sheet", Microfluidics and Nanofluidics, 17(3), pp. 591–604, 2014. https://doi.org/10.1007/s10404-013-1326-2

[10] Ibrahim W., Gadisa, G. "Finite Element Method Solution of Boundary Layer Flow of Powell-Eyring Nanofluid over a Nonlinear Stretching Surface", Journal of Applied Mathematics, 2019(1), 3472518, 2019. https://doi.org/10.1155/2019/3472518

[11] Tshivhi, K. S., Makinde, O. D. "Magneto-nanofluid coolants past heated shrinking/stretching surfaces: Dual solutions and stability analysis", Results in Engineering, 10, 100229, 2021. https://doi.org/10.1016/j.rineng.2021.100229

[12] Fang, T. "Boundary layer flow over a shrinking sheet with power-law velocity", International Journal of Heat and Mass Transfer, 51(25–26), pp. 5838–5843, 2008. https://doi.org/10.1016/j.ijheatmasstransfer.2008.04.067

[13] Postelnicu, A., Pop, I. "Falkner–Skan boundary layer flow of a power-law fluid past a stretching wedge", Applied Mathematics and Computation, 217(9), pp. 4359–4368, 2011. https://doi.org/10.1016/j.amc.2010.09.037

[14] Jalil, M., Asghar, S., Mushtaq, M. "Analytical solutions of the boundary layer flow of power-law fluid over a power-law stretching surface", Communications in Nonlinear Science and Numerical Simulation, 18(5), pp. 1143–1150, 2013. https://doi.org/10.1016/j.cnsns.2012.09.030

[15] Mustafa, I., Shahbaz, S., Usman, Ghaffari, A., Muhammad, T. "Non-similar solution for a power-law fluid flow over a moving wedge", Alexandria Engineering Journal, 75, pp. 287–296, 2023. https://doi.org/10.1016/j.aej.2023.05.077

[16] Shah, Z., Asghar, A., Ying, T. Y., Lund, L. A., Alshehri, A., Vrinceanu, N. "Numerical investigation of sodium alginate-alumina/copper radiative hybrid nanofluid flow over a power law stretching/shrinking sheet with suction effect: A study of dual solutions", Results in Engineering, 21, 101881, 2024. https://doi.org/10.1016/j.rineng.2024.101881

[17] Ahmed, J., Bourazza, S., Sarfraz, M., Orsud, M. A., Eldin, S. M., Askar, N. A., Elkotb, M. A. "Heat transfer in Jeffrey fluid flow over a power law lubricated surface inspired by solar radiations and magnetic flux", Case Studies in Thermal Engineering, 49, 103220, 2023. https://doi.org/10.1016/j.csite.2023.103220

[18] Al-hanaya, A., Rashed, Z. Z., Ahmed, S. E. "Radiative flow of temperature-dependent viscosity power-law nanofluids over a truncated cone saturated heat generating, porous media: Impacts of Arrhenius energy", Case Studies in Thermal Engineering, 53, 103874, 2024. https://doi.org/10.1016/j.csite.2023.103874

[19] Cortell, R. "Viscous flow and heat transfer over a nonlinearly stretching sheet", Applied Mathematics and Computation, 184(2), pp. 864–873, 2007. https://doi.org/10.1016/j.amc.2006.06.077

[20] Tshivhi, K. S., Tshehla, M. S. "Heat source and radiation effect on MHD flow of Copper-Water nanofluid over exponential stretching surface with slip", Results in Physics, 58, 107463, 2024. https://doi.org/10.1016/j.rinp.2024.107463

[21] Yang, D., Israr Ur Rehman, M., Hamid, A., Ullah, S. "Multiple Solutions for Stagnation-Point Flow of Unsteady Carreau Fluid along a Permeable Stretching/Shrinking Sheet with Non-Uniform Heat Generation", Coastings, 11(9), 1012, 2021. https://doi.org/10.3390/coatings11091012

[22] Muhammad, T., Waqas, H., Farooq, U., Alqarni, M. S. "Numerical simulation for melting heat transport in nanofluids due to quadratic stretching plate with nonlinear thermal radiation", Case Studies in Thermal Engineering, 27, 101300, 2021. https://doi.org/10.1016/j.csite.2021.101300

[23] Mandal, I. C., Mukhopadhyay, S. "Nonlinear Convection in Micropolar Fluid Flow Past a Non-Isothermal Exponentially Permeable Stretching Sheet in Presence of Heat Source/Sink", Thermal Engineering, 67(4), pp. 202–215, 2020. https://doi.org/10.1134/S0040601520040059

[24] Ghosh, S., Mukhopadhyay, S. "Flow and heat transfer of nanofluid over an exponentially shrinking porous sheet with heat and mass fluxes", Propulsion and Power Research, 7(3), pp. 268–275, 2018. https://doi.org/10.1016/j.jppr.2018.07.004

[25] Hamid, A., Hashim, Khan, M., Hafeez, A. "Unsteady stagnation-point flow of Williamson fluid generated by stretching/shrinking sheet with Ohmic heating", International Journal of Heat and Mass Transfer, 126, pp. 933–940, 2018. https://doi.org/10.1016/j.ijheatmasstransfer.2018.05.076

[26] Kaur, R., Sharma, S., Chandra, A. "Effects of viscous dissipation, temperature dependent thermal conductivity, and local thermal non-equilibrium on the heat transfer in a porous channel to Casson fluid", The Canadian Journal of Chemical Engineering, 102(11), pp. 3744–3755, 2024. https://doi.org/10.1002/cjce.25459

[27] Ishak, A. "Dual solutions in the stagnation-point flow over a shrinking sheet", International Journal of Mathematical Models and Methods in Applied Sciences, 12, pp. 56–59, 2018.

[28] Mohd Nasir, N. A. A., Ishak, A., Pop, I. "Stagnation-point flow and heat transfer past a permeable quadratically stretching/shrinking sheet", Chinese Journal of Physics, 55(5), pp. 2081–2091, 2017. https://doi.org/10.1016/j.cjph.2017.08.023